# **Diagnosing Diapycnal Mixing from Passive Tracers**

XIAOZHOU RUAN<sup>a</sup> AND RAFFAELE FERRARI<sup>a</sup>

<sup>a</sup> Department of Earth, Atmospheric, and Planetary Sciences, Massachusetts Institute of Technology, Cambridge, Massachusetts

(Manuscript received 16 August 2020, in final form 13 November 2020)

ABSTRACT: Turbulent mixing across density surfaces transforms abyssal ocean waters into lighter waters and is vital to close the deepest branches of the global overturning circulation. Over the last 20 years, mixing rates inferred from in situ microstructure profilers and tracer release experiments (TREs) have provided valuable insights in the connection between small-scale mixing and large-scale ocean circulation. Problematically, estimates based on TREs consistently exceed those from collocated in situ microstructure measurements. These differences have been attributed to a low bias in the microstructure estimates that can miss strong, but rare, mixing events. Here we demonstrate that TRE estimates can suffer from a high bias, because of the approximations generally made to interpret the data. We first derive formulas to estimate mixing from the temporal growth of the second moment of a tracer patch by extending Taylor's celebrated formula to account for both density stratification and variations in mixing rates. The formulas are validated with tracers released in numerical simulations of turbulent flows and then used to discuss biases in the interpretation of TREs based estimates and how to possibly overcome them.

KEYWORDS: Diapycnal mixing; Diffusion; Turbulence; Mixing; In situ oceanic observations; Tracers

#### 1. Introduction

The ocean's meridional overturning circulation (MOC) regulates Earth's climate on centennial to millennial time scales through the transport of vast amounts of carbon, heat, and nutrients (Wunsch 2017). While the upper branch of the MOC is thought to be primarily controlled by wind and buoyancy forcing at the ocean surface (Marshall and Radko 2003; Marshall and Speer 2012), the lower branch requires interior mixing with overlying waters to balance the surface buoyancy loss around Antarctica (Lumpkin and Speer 2007; Talley 2013; Ferrari 2014). The key role played by turbulent mixing across density surfaces—diapycnal mixing—in maintaining the vertical buoyancy balance in the global ocean was already recognized by Stommel and Arons (1959) and Munk (1966), yet its accurate quantification remains elusive till today.

In the absence of observations, diapycnal mixing was first assumed to be uniform throughout the ocean interior resulting in a uniform upwelling of abyssal waters toward the ocean surface (Stommel and Arons 1959; Munk 1966). Field campaigns over the last two decades revealed that diapycnal mixing is very variable, being weak in most of the ocean interior and increasing by orders of magnitude close to rough bathymetry (Polzin et al. 1997; Waterhouse et al. 2014). These observations have led to the hypothesis that upwelling of abyssal waters is confined to thin bottom boundary layers along sloping topography, where the diapycnal mixing generates a convergent buoyancy flux or equivalently an increase in buoyancy. A compensating downwelling of abyssal waters crossing density surfaces is then posited to occur above the upwelling flow where the mixing-driven buoyancy flux is divergent—waters are mixed more vigorously with the less buoyant waters below than with the more buoyant waters above as a result of the

increase in mixing rates with depth (Ferrari et al. 2016; de Lavergne et al. 2016). In this view, the spatial distribution of turbulent mixing is crucial for determining the water pathways in the abyssal ocean (Callies and Ferrari 2018).

It is very challenging to measure diapycnal mixing in the ocean, because it is associated with internal wave breaking events spanning a few meters and other small-scale turbulent processes, while its impact is felt on basin scales of thousands of kilometers. Free-falling microstructure profilers are believed to be the most accurate platforms to measure vertical profiles of mixing at one location in the ocean, while tracer release experiments (TREs) best quantify the net mixing experienced by the tracer cloud over a large patch of ocean. Diapycnal mixing rates are often reported as a diapycnal diffusivity  $\kappa$ , which quantifies the local rate at which turbulence spreads a tracer across density surfaces. Microstructure profilers record in situ high-frequency temperature and velocity variance which are then converted into a diapycnal diffusivity under various assumptions about the turbulence statistics (Osborn and Cox 1972; Osborn 1980). The TREs instead measure the diapycnal diffusivity as the rate at which a tracer spreads across density surfaces, while being stirred along density surfaces over areas easily spanning thousands of kilometers (Ledwell and Bratkovich 1995; Ledwell et al. 2000). Releasing a tracer and sampling its spread over months, if not years, is very expensive but overcomes both the limited spatial sampling and the assumptions about turbulence statistics underlying the microstructure profile measurements. A combination of the two approaches is clearly desirable, but the conversion from tracer spreading to a diapycnal diffusivity is challenging when the intensity of turbulent mixing varies rapidly, like close to rough bathymetry.

A few experiments tackled the measurement of diapycnal diffusivities with both microstructure profilers and TREs. The TRE based estimates have typically exceeded those based on in situ microstructure profiles, particularly in the abyssal ocean

Corresponding author: Xiaozhou Ruan, xruan@mit.edu

and over complex topography (Ledwell et al. 1998, 2000; Watson et al. 2013). These discrepancies have been attributed to a sampling bias in the microstructure profiles, which would have missed strong mixing events associated with different physics in each experiment (e.g., double diffusion, tidal mixing, boundary layer processes, etc.). We suggest that an additional, and independent, source of bias comes from approximations often made to infer diapycnal diffusivities from TREs. This is demonstrated by deriving exact formulas to compare the diapycnal diffusivity inferred from the spreading of a tracer from that estimated with in situ measurements. The new formulas can be seen as an extension of Taylor's formula (Taylor 1922) to the case where 1) the diapycnal diffusivity is not constant and 2) the fluid is stratified, two crucial aspects when considering diapycnal mixing in the ocean. The accuracy of the new formulas is verified with idealized simulations where we release a numerical tracer in a stratified fluid with a variable  $\kappa$  profile and a strong geostrophic eddy field. We demonstrate that traditional approximations used to interpret TRE results lead to an overestimate of  $\kappa$ .

The paper is organized as follows: we first introduce our theoretical framework for diagnosing diapycnal diffusivity from passive tracers in section 2; the setup of the numerical simulations is described in section 3, followed by validation of the theoretical framework in section 4; discussions and conclusions are provided in sections 5 and 6.

### 2. Theory

Taylor (1922) in a seminal paper considered the evolution of a tracer of concentration c experiencing a constant turbulent diffusivity  $\kappa$  according to the equation

$$\partial_{\cdot} c = \kappa \nabla^2 c. \tag{1}$$

He demonstrated that the diffusivity  $\kappa$  can be estimated from the growth rate of the second moment of the tracer in any direction, for example the vertical direction,

$$\kappa = \frac{1}{2} \frac{\partial_t \iiint z^2 c \, dx \, dy \, dz}{\iiint c \, dx \, dy \, dz},\tag{2}$$

where the integral is taken over the full volume of the fluid.

Equation (2) has been the inspiration for TREs. A tracer is released in the ocean, and its vertical spreading is measured over time in order to infer the vertical diffusivity as a proxy of the diapycnal diffusivity, because density surfaces are to leading order flat. However, a number of complications arise in ocean settings compared to the problem considered by Taylor: the turbulent diffusivity is not constant, and the tracer is advected by large-scale motions in addition to being diffused by small-scale turbulence. Here we describe a new approach that extends Taylor's work by including these effects. Our goal is to estimate the turbulent diffusivity  $\kappa$  associated with instabilities that mix buoyancy and tracers across density surfaces, typically breaking waves, but also hydraulic jumps, bores and other hydrodynamic instabilities, with spatial scales of tens to

hundreds of meters and temporal scales of minutes to hours (Ferrari and Wunsch 2009). Oceanic motions on larger scales do not overturn density surfaces, because the stabilizing effects of stratification and rotation constrain these larger flows along density surfaces. It is therefore useful to focus the analysis on tracer diffusion across density surfaces (diapycnal diffusion) so as to eliminate the along-density stirring by larger-scale motions

We begin by writing the full conservation equations for a tracer of concentration c and buoyancy b, averaged over spatial and temporal scales larger than those characteristic of breaking internal waves or other diapycnal turbulent processes,

$$\partial_{c}c + \mathbf{u} \cdot \nabla c = \nabla \cdot (\kappa \nabla c), \tag{3}$$

$$\partial_{\cdot} b + \mathbf{u} \cdot \nabla b = \nabla \cdot (\kappa \nabla b). \tag{4}$$

Buoyancy is defined as  $b = -g\gamma'/\rho_0$ , where  $\rho_0$  is a reference in situ density and  $\gamma'$  is the neutral density (Jackett and McDougall 1997) departure from its mean; buoyancy and density are therefore linearly proportional and will be used interchangeably. We ignore nonlinearities in the equation of state which contribute additional terms to the right hand side of Eq. (4), because they are not likely to matter at the regional scales considered in TREs, but they could be included in regions where they become significant, like in the Southern Ocean (Klocker and McDougall 2010). We further assume that the diffusivity tensor is isotropic,  $\kappa_{ij} = \kappa \delta_{ij}$ , with  $\delta_{ij}$  the Kronecker delta, and the magnitude of the diffusivity is spatially variable  $\kappa = \kappa(x, y, z, t)$ .

To describe the spreading of a tracer across density surfaces, it is useful to introduce the tracer-weighted buoyancy moments. We define the tracer-weighted average operator as

$$\overline{(\cdot)} = \frac{\iiint(\cdot) c \, dx \, dy \, dz}{\iiint c \, dx \, dy \, dz}, \tag{5}$$

where the integral is carried over the whole ocean volume. We will consider the evolution of the first buoyancy moment  $\overline{b}$  and the centered second buoyancy moment  $\overline{(b-\overline{b})}^2$ . The first moment represents the centroid of tracer in buoyancy space, i.e., the mean buoyancy class occupied by the tracer. The centered second moment, instead, describes the spread of tracer about the first moment. The temporal evolution of these two moments describe the drift and thickening of a tracer cloud across density surfaces.

The evolution equation for the *n*th buoyancy moment  $\overline{b^n}$  is derived by first multiplying Eq. (3) by  $b^n$  and Eq. (4) by  $ncb^{n-1}$ , summing them up and taking the volume average (see appendix A). The evolution equation for the first buoyancy moment is given by

$$\partial_{\cdot} \overline{b} = 2 \overline{\nabla \cdot (\kappa \nabla b)} = 2 \overline{\omega}. \tag{6}$$

Equation (6) holds for no normal flow boundary conditions, no tracer and buoyancy fluxes through solid boundaries and either no tracer concentration or no buoyancy flux at the ocean surface. The buoyancy velocity  $\omega = Db/Dt = \nabla \cdot (\kappa \nabla b)$  is defined

in analogy to the vertical velocity w = Dz/Dt.<sup>1</sup> The surprising result that the first moment rises/sinks at twice the buoyancy velocity is because both Dc/Dt and Db/Dt evolve in response to the same diapycnal diffusivity and therefore their product D(cb)/Dt evolves at twice that rate.

The evolution equation for the second buoyancy moment is

$$\partial_{t}\overline{b^{2}} = 2\overline{\kappa |\nabla b|^{2}} + 4\overline{\omega b}, \qquad (7)$$

valid under the same boundary conditions assumed for the first moment. To separate the second-moment growth due to the mean drift of the tracer across density surfaces from that due to the tracer spreading around its centroid, we write the evolution equation for the centered second moment obtained combining Eqs. (6) and (7),

$$\partial_{t}\overline{(b-\overline{b})^{2}} = 2\overline{\kappa |\nabla b|^{2}} + 4(\overline{\omega b} - \overline{\omega}\overline{b}).$$
 (8)

The first term on the right-hand side of Eq. (8) represents the spreading of tracer identified by Taylor and is proportional to the magnitude of local diffusivity  $\kappa$ , while the second term represents the spreading induced by diapycnal changes in the buoyancy velocity. This term is best written as  $4\overline{\omega'b'}$ , i.e., the correlation between departures of  $\omega$  from its tracer-weighted mean and b'. If the buoyancy velocity experienced by the tracer increases toward heavier waters (lower buoyancy values), then the heavy tail of the tracer will sink more rapidly than the light tail resulting into an increase in the tracer spread about the first moment. This is illustrated in Fig. 1 which shows the development of a skewed tail in the tracer distribution toward lower buoyancy.

It is useful to convert the moment formulas into expressions for a tracer-based diapycnal velocity and diffusivity acting on the mean buoyancy gradient. This is done by dividing Eqs. (6) and (8) by the buoyancy gradient and the buoyancy gradient squared, respectively:

$$W_{\text{tracer}} = \frac{1}{2} \frac{\partial_t \overline{b}}{|\nabla b|} \simeq \frac{\overline{\omega}}{\partial_z \overline{b}},\tag{9}$$

$$K_{\text{tracer}} = \frac{1}{2} \frac{\partial_t \overline{(b - \overline{b})^2}}{\overline{|\nabla b|^2}} \simeq \underbrace{\frac{\overline{\kappa (\partial_z b)^2}}{\underline{(\partial_z b)^2}}}_{K_{\text{Taylor}}} + 2\underbrace{\frac{\overline{\omega' b'}}{(\partial_z b)^2}}_{K_{\omega}}, \quad (10)$$

where we approximated the 3D buoyancy gradients with their vertical components. This is an excellent approximation in the ocean interior at scales above a few tens of meters, the scales at which these equations are supposed to apply. However, the full 3D buoyancy gradients ought to be used if the horizontal components are not negligible, such as near steep topographic slopes.

The interpretation of  $W_{\rm tracer}$  as the diapycnal velocity of the centroid of a tracer patch is straightforward. The interpretation of  $K_{\rm tracer}$  is instead more nuanced. If the buoyancy velocity

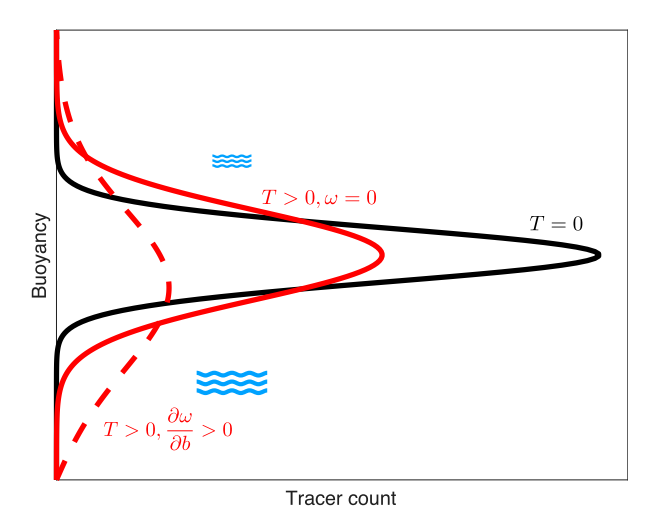


FIG. 1. Schematic of the evolution of tracer distribution in buoyancy space. The black line denotes an initial standard normal distribution. The solid red line is a later time distribution in a homogeneous environment where the variance increases symmetrically around the mean. The dashed red line is a skewed distribution at the same time of the solid red line but in an inhomogeneous environment where mixing (blue curly lines) is stronger at lower buoyancy region.

 $\omega$  and the turbulent diffusivity  $\kappa$  are constant, then one recovers the result in Taylor (1922) that  $K_{\text{tracer}} = \kappa$ . However, more generally,  $K_{\text{tracer}}$  is the result of two separate contributions:  $K_{\text{Taylor}}$  and  $K_{\omega}$ . Consider a tracer patch released at some depth in the ocean interior. The contribution  $K_{\text{Taylor}}$  captures the dispersion of the patch induced by the local turbulent diffusivity, weighted by  $(\partial_z \overline{b})^2$  to account for the faster diapycnal spreading where the stratification is larger. The part  $K_{\omega}$ , instead, results from variations in the buoyancy velocity which act to stretch the tracer patch across buoyancy surfaces. For example, an  $\omega$  profile decreasing toward the ocean bottom, where buoyancy is smaller than  $\overline{b}$ , would result in a tracer profile developing a skewed tail toward lower buoyancy and thus a growing second moment (see Fig. 1).

Microstructure profiles have provided unquestionable evidence that above rough bathymetry turbulent mixing rapidly intensifies toward the seafloor resulting in a negative buoyancy velocity,  $\omega = \partial_z(\kappa \partial_z \overline{b}) < 0$ , whose magnitude increases exponentially toward the seafloor (Polzin et al. 1997; Waterhouse et al. 2014). In a stably stratified fluid this results in smaller  $\omega$  for lower b and thus a positive  $K_\omega$ . Numerical simulations described below, and field campaign results show that  $K_\omega$  can be as large as  $K_{\rm Taylor}$  in the abyssal ocean, where mixing is strong and bottom intensified, and can contribute to making  $K_{\rm tracer} \gg \kappa$ .

A second important implication of Eqs. (9) and (10) is that correlations between tracer concentration c and  $\kappa$ ,  $\omega$ , and  $\partial_z b$  result in larger  $W_{\text{tracer}}$  and  $K_{\text{tracer}}$ . Such correlations can be anticipated, because tracers preferentially diffuse toward larger  $\kappa$  values and sink toward larger  $\omega$  values, when other constraints or isopycnal flows are absent. As we review below, the sparse tracer sampling in TREs makes it difficult to

<sup>&</sup>lt;sup>1</sup> D/Dt is the Lagrangian derivative  $D/Dt \equiv \partial_t + \mathbf{u} \cdot \nabla$ .

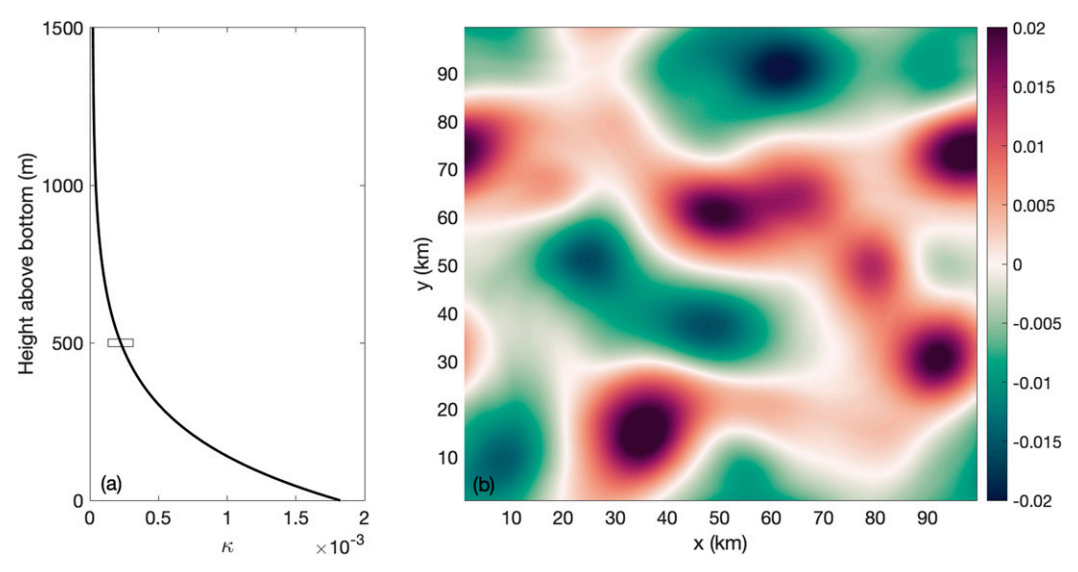


FIG. 2. Prescribed diffusivity profile and the vorticity field at the beginning of the tracer release. (a) The prescribed diffusivity profile in the inhomogeneous run is shown, with the gray box indicating the location of the tracer injection. (b) Relative vorticity  $(\zeta = \partial_x v - \partial_y u)$  normalized by the Coriolis frequency f at HAB = 500 m at the tracer injection. This relative vorticity distribution is the same for both runs after the spinup.

quantify these correlations, which may explain the difference between microstructure and tracer-based estimates of mixing.

#### 3. Numerical simulations

A pair of idealized numerical simulations are performed with the Massachusetts Institute of Technology general circulation model (MITgcm) (Marshall et al. 1997) to simulate oceanic flows with a strong eddy field. Numerical tracers are released in these flows and the formulas derived in the previous section are used to quantify the diapycnal velocity and diffusivity experienced by the tracer.

The model is configured in a doubly periodic box with a flat bottom with a horizontal resolution of 500 m and a vertical resolution of 3 m. For simplicity, buoyancy is assumed to be a linear function of temperature only and the simulations start with a constant vertical stratification of  $N^2 = 1 \times 10^{-6} \, \text{s}^{-2}$ . To produce an active meso/submesoscale flow field, the two simulations are spun up with an initial sinusoidal buoyancy/temperature perturbation in the *y* direction as a potential energy reservoir for baroclinic instability (see Fig. 2 and appendix B). The vertical viscosity is constant and equal to  $\nu = 5 \times 10^{-4} \, \text{m}^2 \, \text{s}^{-1}$ . The Coriolis frequency is set to  $f = 1 \times 10^{-4} \, \text{s}^{-1}$ . To prevent the bottom stratification from being eroded away by the no flux bottom boundary condition, the stratification is restored back to its initial value in a sponge layer of 400 m thick at the bottom of the model domain (appendix B).

One simulation (experiment A) uses a constant vertical/diapycnal diffusivity  $\kappa = 2 \times 10^{-5} \, \text{m}^2 \, \text{s}^{-1}$ , and the other (experiment B) a bottom intensified profile (Fig. 2a),

$$\kappa = \kappa_0 + \kappa_1 \, e^{-z/h} \,, \tag{11}$$

where the bottom is at z = 0,  $\kappa_0 = 2 \times 10^{-5}$  m<sup>2</sup> s<sup>-1</sup>,  $\kappa_1 = 1.8 \times 10^{-3}$  m<sup>2</sup> s<sup>-1</sup>, and h = 230 m. The two profiles are inspired by

realistic, but distinct, oceanic environments. The constant diffusivity run aims to mimic the ocean thermocline, where mixing is weak and uniform (Ledwell and Bratkovich 1995). The bottom intensified profile is based on those measured in the Brazil Basin over the Mid-Atlantic Ridge where the diapycnal diffusivity increased dramatically toward the seafloor (Polzin et al. 1997; Ledwell et al. 2000; Polzin 2009). Both field experiments are reviewed in more detail below. Despite the difference in the diffusivity profiles, the horizontal velocity fields and their shears are very similar in the two runs because the stratification is quite similar in the two simulations as a result of the restoring imposed in the bottom layer.

### 4. Results

After an initial spinup during which the simulations develop a vigorous eddy field, a numerical tracer is released in each simulation 500 m above the bottom—the above-bottom depth at which a chemically inert tracer was released in the Brazil Basin Tracer Release Experiment (BBTRE) field campaign. The tracer patch starts as a Gaussian with standard deviations of 10 m in the vertical and 10 km in both horizontal directions. The evolution of the tracer blob is followed for 180 days, by which time the tracer filaments span the whole domain in the horizontal (Fig. 3). While eddies stir the tracer along density surfaces, the turbulent diffusivity spreads the tracer across density surfaces. Our goal is to estimate the rate of diapycnal spreading experienced by the tracer cloud using the diapycnal velocity  $W_{\rm tracer}$  and diffusivity  $K_{\rm tracer}$  diagnostics given by Eqs. (9) and (10).

Figure 4 compares the temporal evolution of the left hand side of Eq. (9),  $W_{\rm tracer}$ , with the right-hand side,  $\overline{\omega}/\partial_z \overline{b}$ . The comparison is repeated for both experiments A (blue line and dots) and B (red line and dots). Time derivatives are computed

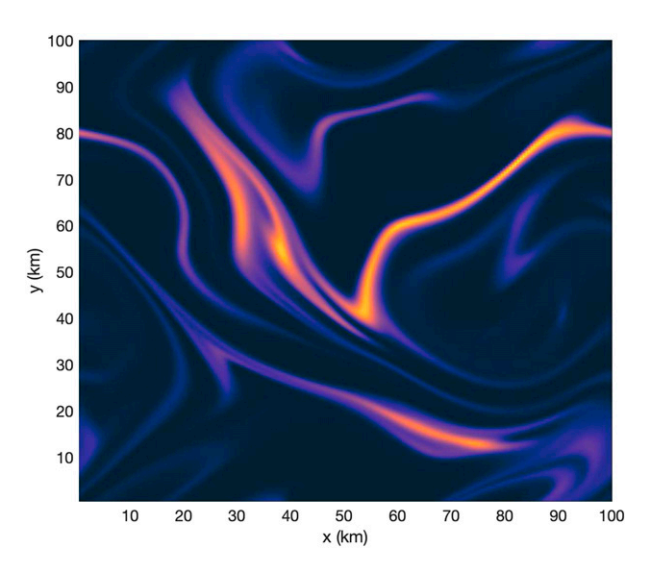


FIG. 3. The vertically integrated tracer concentration at the end of the 180-day run for experiment B. The distribution is similar in experiment A because of the similar dynamic field.

over 5-day intervals. In both cases the two terms lie on top of each other supporting the approximation of the full buoyancy gradient by its vertical component. In experiment A, the diapycnal velocity is essentially zero, because the vertical buoyancy flux,  $\kappa \partial_z \overline{b}$ , is constant and thus  $\overline{\omega} \simeq 0$ . In experiment B, instead, the tracer sinks at a rate of 9 cm day<sup>-1</sup> at the beginning of the simulation and up to nearly 12 cm day<sup>-1</sup> after 180 days as the tracer patch sinks to depths where the divergence of buoyancy flux becomes larger.

Next, we estimate  $K_{\text{tracer}}$  from experiments A and B using the rate of change of the centered second moment. In experiment A,  $K_{\text{Tracer}}$  and  $K_{\text{Taylor}}$  are constant in time and equal (figure not shown; see Table 1 for the results at day 180) as expected, because  $\omega$  and hence  $K_{\omega}$  are zero (see Fig. 4). In experiment B,  $K_{\text{Tracer}}$  is larger than  $K_{\text{Taylor}}$ , because there is a downward diapycnal velocity which increases with depth and thus generates a substantial correlation between  $\omega$  and b resulting in a large  $K_{\omega}$ . The discrepancy increases in time as the centroid of the tracer sinks to denser water where  $K_{\omega}$  is larger (Fig. 5a). At the end of the 180-day run,  $K_{\text{Tracer}}$  exceeds  $K_{\text{Taylor}}$ by 36% (Table 1). We also show that  $K_{\text{Taylor}}$  is well approximated by the tracer-weighted diffusivity  $\bar{\kappa}$  (Fig. 5a and Table 1), a metric that has been used to compare the diapycnal diffusivity from microstructure profile measurements with that based on tracer spreading; the only difference between  $K_{\text{Taylor}}$ and  $\overline{\kappa}$  is that the former weighs  $\kappa$  values both by tracer concentration and stratification, while the latter weighs only by tracer concentration. The result that  $K_{\text{Taylor}} \simeq \overline{\kappa}$  is not surprising given the small changes in stratification in our simulations, but it may not hold in environments where stratification is variable.

The along-isopycnal averaged tracer distribution from experiment B nicely illustrate how a diapycnal velocity increasing toward the seafloor impacts the diapycnal spreading of the tracer. The tracer concentration in both buoyancy and depth

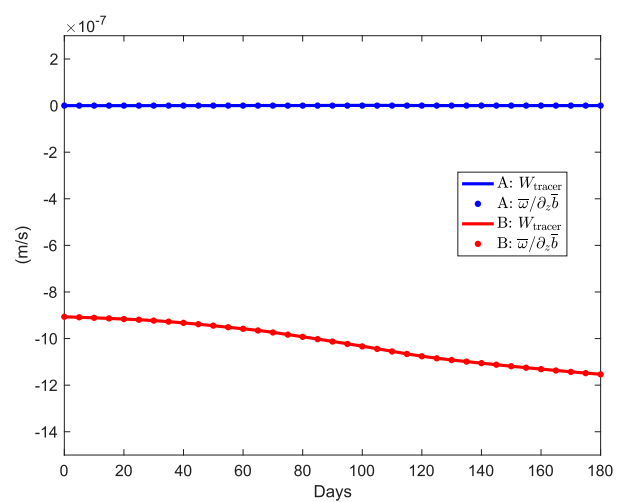


FIG. 4. The diagnosed  $W_{\text{tracer}}$  and  $\overline{\omega}/\partial_z \overline{b}$  in Eq. (9) for both experiments.

above the bottom (equivalent to depth here as the bottom is flat) develops a skewness toward denser waters as shown in Figs. 5b and 5c and consistent with the schematic in Fig. 1. A similar skewness has also been reported in TREs (Ledwell et al. 2000).

In practice, tracer surveys and sampling are separated by months or years due to ship time constraints, so the spreading rate of the tracer cannot be computed at 5-day intervals as done in this study. We therefore estimated  $K_{\rm Tracer}$  from Eq. (10) taking the time derivative of the second moment as the difference between t=0 and t=180 days and using the stratification at the injection location. Instead  $\overline{\kappa}$  was evaluated at the end of the simulation. This exercise returned  $K_{\rm Tracer} \simeq 3.2 \times 10^{-4} \, {\rm m}^2 \, {\rm s}^{-1}$  and 23% larger than  $\overline{\kappa} = 2.6 \times 10^{-4} \, {\rm m}^2 \, {\rm s}^{-1}$ .

In experiments A and B,  $\kappa$  is horizontally uniform and the stratification is nearly constant both in the horizontal and vertical directions, so no lateral correlations can develop between the tracer concentration and either  $\kappa$  or  $\omega$ . Such correlations can, however, develop if 1) the tracer experiences different diapycnal mixing rates in different subregions and 2) the lateral homogenization time scale by eddy stirring is longer than the time scale over which the diapycnal spreading is observed. We could run a numerical simulation over such a large domain that lateral homogenization did not occur over the 180 days of simulation. However, a much simpler and computationally cheaper strategy is to assume that experiment A and B represents two parts of a single tracer patch sufficiently separated in the horizontal to be brought in contact by lateral

TABLE 1. Summary of the diagnosed diffusivity at day 180. The K values are calculated in 5-day intervals, and  $\kappa$  values are taken from the last snapshot (units are  $\times 10^{-4}\,\mathrm{m}^2\,\mathrm{s}^{-1}$ ).

	$K_{\mathrm{tracer}}$	$K_{\mathrm{Taylor}}$	$K_{\omega}$	$\overline{\kappa}$
Expt A	0.20	0.20	0.0	0.20
Expt B	3.65	2.69	0.95	2.63

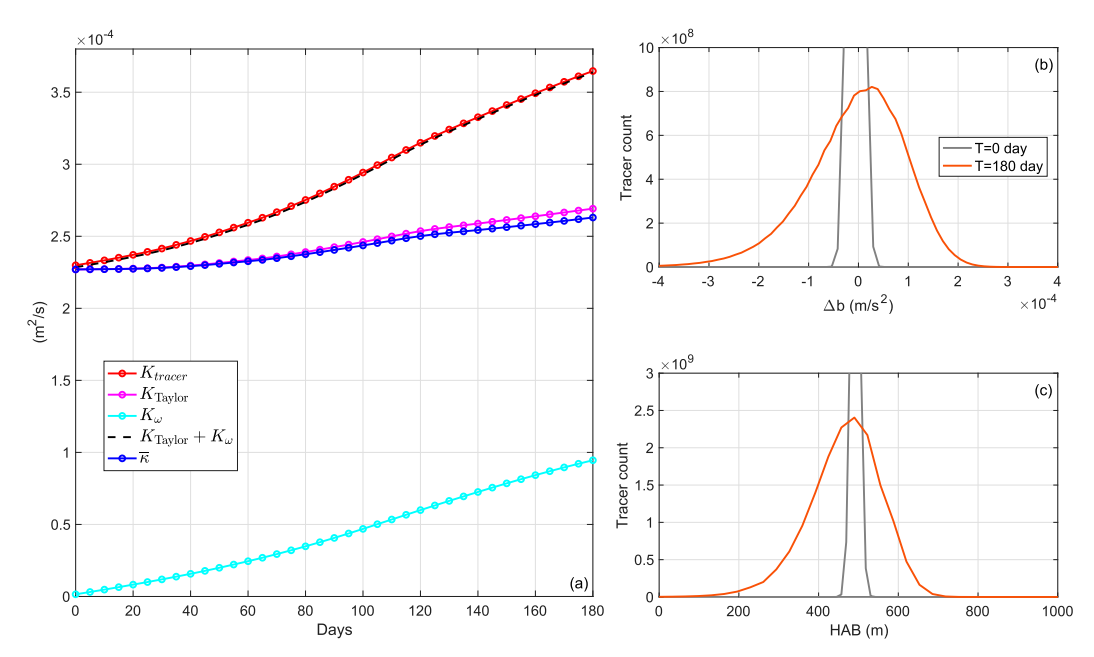


FIG. 5. Diapycnal mixing diagnostics for experiment B. (a) Diagnosed diapycnal diffusivity based on Eq. (10). The red line is  $K_{\text{Tracer}}$ , while the purple and cyan lines are the  $K_{\text{Taylor}}$  and  $K_{\omega}$  contributions whose sum (black dashed line) matches the red line. The blue line is the tracer averaged diffusivity. (b) The distribution of tracer concentration in buoyancy space.  $\Delta b$  is defined as  $b - \overline{b}$ , i.e., the buoyancy departure from the first buoyancy moment. Note that the maximum of the tracer concentration shifts toward positive  $\Delta b$  not because the tracer has moved toward lighter density classes, but rather because  $\overline{b}$  decreases as a result of the skewed tail in the tracer distribution. (c) The distribution of tracer concentration as a function of HAB.

stirring. Experiment A would then represent the fraction of tracer that ends up far from topography and thus experiences weak mixing, while experiment B would represent the fraction that comes close to rough bathymetry, where mixing is strong. The diffusivity of the whole patch would be given by

$$K_{\text{tracer}} = \frac{\overline{\kappa(\partial_z b)^2}^A + \overline{\kappa(\partial_z b)^2}^B}{\overline{(\partial_z b)^2}^A + \overline{(\partial_z b)^2}^B} + 2\frac{\overline{\omega' b'}^A + \overline{\omega' b'}^B}{\overline{(\partial_z b)^2}^A + \overline{(\partial_z b)^2}^B}, \quad (12)$$

where the superscripts denote volume integrals on the fraction of tracers represented by experiments A and B<sub>2</sub> respectively. Dividing numerators and denominators by  $(\partial_z b)^2$  we then obtain

$$K_{\text{tracer}} = \frac{K_{\text{tracer}}^A + \delta K_{\text{tracer}}^B}{1 + \delta},$$
 (13)

where  $\delta = \overline{(\partial_z b)^2}^B/\overline{(\partial_z b)^2}^A$  and  $K_{\rm tracer}^A$  and  $K_{\rm tracer}^B$  are the diffusivities obtained restricting the integrals to regions A or B only. In our simulations where the stratification is constant in the vertical and equal in the two experiments,  $\delta$  reduces to the ratio of the total amount of tracer in region B over that in region A. If there is an equal amount of tracer in the two regions, then  $\delta = 1$  and the diffusivity experienced by the total tracer patch,  $K_{\rm tracer}$ , is the average of those estimated separately in the two regions,  $K_{\rm tracer}^A$  and  $K_{\rm tracer}^B$ . Otherwise,  $K_{\rm tracer}$  will be closer to that in the region with larger integrated tracer amount.

We can now explore how correlations between tracer concentration and  $\kappa$  and/or  $\omega$  affect  $K_{tracer}$ . In a typical TRE, the

volume occupied by tracer experiencing weak mixing is much larger than that occupied by tracer experiencing strong mixing, because strong mixing occurs only in limited regions close to rough topography. For the sake of argument, let us assume that the volume of region A is 10 times larger than 10 of region B. If the tracer concentration is the same in the two regions, and therefore there is no correlation between c and either  $\kappa$  or  $\omega$ , then  $\delta = 0.1$  and  $K_{\text{Tracer}} \simeq K_{\text{Tracer}}^A$ . However, if c is larger in region B where mixing is strong, and therefore there is a positive tracer correlation between c and either or both  $\kappa$  and  $\omega$ , then  $\delta > 0.1$ . Figure 6 shows how  $K_{\text{Tracer}}$  grows for increasing  $\delta$  using  $K_{\text{tracer}}^A$  and  $K_{\text{tracer}}^B$  from simulations A and B at day 180. The impact of the strong mixing region becomes progressively more important as  $\delta$  increases above one, i.e., when the tracer concentration in region B becomes more than 10 times larger than that in region A (still assuming that the ratio of volumes occupied by the tracer in regions B and A is 0.1);  $K_{\text{tracer}}$  grows by up to a factor of 6 for  $\delta = 0.1$  (Fig. 6). Given that tracers tend to diffuse toward regions of large  $\kappa$  and sink toward region of large  $\omega$ , in the absence of other flows, one may anticipate that  $\delta$  does exceed one in many settings; a clear example will be presented in the next section. This simple thought experiment confirms that estimates from in situ microstructure profiles, which typically estimate diffusivities as the average of all available profiles and thus ignore the potential dominance of regions where the tracer concentration is largest (making  $\delta$  larger than one there), may be biased low compared to tracer-based estimates, which by definition account for tracer concentration.

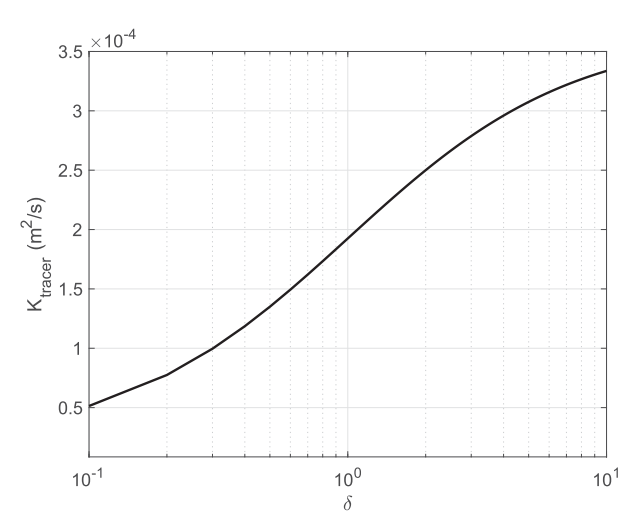


FIG. 6. Shown is  $K_{\text{tracer}}$  as a function of  $\delta$ , the ratio of the total tracer amount in strong bottom enhanced vs weak uniform mixing regions, estimated using Eq. (13).

Our simulations after the tracer release last for 180 days, much shorter than the typical duration of actual TREs (1-2 years) in field campaigns. Thus, the discrepancy between  $K_{\text{Tracer}}$  and  $K_{\text{Taylor}}$  will likely increase more rapidly as the tracer cloud sinks to denser regions. In our experiments, the tracer does not get close enough to the seafloor to experience a reduction in spreading due to the no flux boundary condition, an effect emphasized by Holmes et al. (2019). The impact of a solid bottom on tracer would be captured by the equations for the diapycnal velocity and diffusivity which account for the no-flux bottom boundary (appendix A). As the tracer patch reaches the bottom, the tracer-weighted buoyancy would no longer decrease. Instead, it will increase as the upper half of the tracer patch spreads toward lighter waters. This will result in a negative correlation between the buoyancy velocity and buoyancy and thus reduce  $K_{\text{Tracer}}$ .

## 5. Discussions

The new formulas and numerical experiments demonstrated that  $K_{\rm tracer}$  can be larger than a straightforward volume average of the local  $\kappa$  due to two main effects: 1) vertical variations in  $\omega$  and 2) correlations between  $\kappa$ ,  $\omega$ ,  $\partial_z b$ , and the tracer concentration. We now present evidence from two field campaigns that illustrate the importance of the first and second effect respectively. These two campaigns are chosen because they targeted ocean environments with strong variations in mixing rates; both effects vanish in environments with uniform mixing and stratification.

Before discussing the two experiments, it is worth pointing out an important difference between our formulas and the traditional approach used to estimate diapycnal velocities and diffusivities from TREs. Our formulas give bulk estimates of  $\omega$  and  $\kappa$  averaged over the whole volume occupied by the tracer, without assuming any functional forms of the diffusivity profiles. The traditional approach instead relies on solving a

one-dimensional advection-diffusion equation. The profiles of vertical velocity and diffusivity are adjusted to obtain the best match to the temporal evolution of the vertical tracer distribution (averaged along isopycnals). This approach provides an estimate of diapycnal velocity and diffusivity for each density surface, but it does so at the cost of assuming that the tracer concentration c is uniform along each density surface, thereby ignoring possible correlations between c,  $\kappa$ ,  $\omega$ , and  $\partial_z b$ . Our formulas instead take these correlations into account, but at the cost of returning single values averaged over the whole tracer volume. Furthermore, we emphasize that matching the tracer distribution in depth space, especially the ones with large skewness in environments where mixing and background stratification are highly nonuniform, could potentially miss half of the full contribution from vertical variations in  $\omega$  (see appendix C). We illustrate that a combination of diffusivity estimates with both approaches is the best way forward toward resolving the conundrum of why tracers appear to experience more mixing than inferred from microstructure measurements.

There have been two major field campaigns targeting the deep ocean with concurrent tracer and microstructure measurements. In both experiments the diapycnal diffusivity estimated from the TREs exceeded the one estimated from microstructure profiles. We will begin with the BBTRE, which provides a good example for the importance of vertical  $\omega$  variations in setting  $K_{\text{Tracer}}$ . BBTRE targeted a region above the Mid-Atlantic Ridge and provided the first documentation from in situ microstructure observations that deep mixing dramatically increases in the proximity of rough bathymetry (Polzin et al. 1997). The concurrent TRE found that the tracer distribution developed a skewed tail toward higher densities (Ledwell et al. 2000), much like in our idealized numerical experiment B. A vertical diffusivity profile was estimated by minimizing the difference between the observed tracer distribution at 14 months and the solution of a one-dimensional advection-diffusion equation.2 At the depth where the tracer was released, the fit returned a value of  $K = (3 \pm 1) \times$  $10^{-4} \,\mathrm{m}^2 \,\mathrm{s}^{-1}$ . Most importantly for us the advective tracer flux was found to be of the same order as the diffusive tracer flux, consistent with our claim that  $K_{\omega}$  can be comparable to  $K_{\text{Taylor}}$ in regions with strong vertical variations in mixing rates.

A first isopycnal average of the BBTRE microstructure-based diffusivity at the depth where the tracer was released returned a value of 0.3– $0.6 \times 10^{-4} \, \text{m}^2 \, \text{s}^{-1}$ , substantially lower than the tracer based estimate (Polzin et al. 1997). However, the estimate was later updated to  $2.3 \pm 1 \times 10^{-4} \, \text{m}^2 \, \text{s}^{-1}$  after correcting for spatial and temporal biases (Ledwell et al. 2000):

<sup>&</sup>lt;sup>2</sup> Ledwell et al. (2000) solved the one-dimensional equation for the tracer concentration  $\hat{c}$  averaged over an isopycnal surface of area A(z) chosen to encompass the whole tracer at the end of the experiment,  $A\hat{c}_t + \partial_z (Aw\hat{c}) = \partial_z (A\kappa\hat{c}_z)$ , where z was the mean depth of a density surface,  $w = (\partial_z \hat{b})^{-1} \partial_z (AK\partial_z \hat{b})$  was the diapycnal velocity, and K(z) was a prescribed two parameter analytical function. The two parameters were estimated by least squares fitting the solution of the one-dimensional equation to the observed tracer distribution at 14 months.

the sampling targeted deep bathymetry to avoid hitting the seafloor with profilers, thus undersampling regions where the tracer came close to the strong mixing within a few hundred meters of the seafloor. The diffusivity estimates had to be corrected also for the phase of the barotropic tide which strongly modulated mixing rates in the region. While these corrections seemed to have settled discrepancies between the tracer and microstructure estimates, recent work by J. Ledwell (2020, personal communication) suggests that  $K \simeq 4 \times 10^{-4} \, \text{m}^2 \, \text{s}^{-1}$  best fits the observed tracer data. Should this larger estimate be confirmed, our formulas suggest that the discrepancy may be associated with variations in tracer concentrations along the target density surface, which are ignored in the one-dimensional budget used to interpret the tracer data.

The Diapycnal and Isopycnal Mixing Experiment in the Southern Ocean (DIMES) is an even better example of the importance of correlation between tracer concentration and strong mixing. DIMES targeted the middepth of the water column at 1500-m depth, west and east of Drake Passage (St. Laurent et al. 2012; Watson et al. 2013). This depth was a few kilometers above the bottom west of the passage, but about the height of the many ridges and seamounts crossing the passage. The diapycnal diffusivity was inferred from the tracer evolution by solving a 2D advection–diffusion equation,  $c_t + uc_x =$  $Kc_{zz}$ , where u represented advection by the zonal Antarctic Circumpolar Current, taken to be constant, x was the zonal direction, and K(x) had two different values, one west and the other east of Drake Passage (Watson et al. 2013). Using a least squares fit of the 2D solution to tracer profiles measured over the following two years across different latitude-depth sections, it was inferred that east of Drake Passage, where the tracer experienced strong mixing coming close to the seafloor above the numerous ridges and seamounts, K was 3.6  $\pm$  0.6  $\times$  $10^{-4}\,\mathrm{m}^2\,\mathrm{s}^{-1}$  and a full order of magnitude larger than the microstructure estimate of  $3 \times 10^{-5} \,\mathrm{m}^2 \,\mathrm{s}^{-1}$  (Watson et al. 2013; Mashayek et al. 2017).

Mashayek et al. (2017) released a tracer in a numerical simulation of the DIMES region east of Drake Passage where the authors imposed a self-similar  $\kappa$  profile decaying exponentially with height above the bottom fitted to the available microstructure estimates. They found that the tracer accumulated

over shallow topographic features—ridges and seamounts—where mixing was strong. This resulted in a strong correlation between large  $\kappa$  and large c. The accumulation was the result of bottom enhanced mixing driving tracer toward the seafloor where horizontal velocities were weak and thus the tracer accumulated for long times. Mashayek et al. (2017) found that the positive correlation between  $\kappa$  and c explained the discrepancy between tracer and microstructure-based estimates, but this was ignored in the analysis of the DIMES observations for lack of sufficient spatial sampling. The DIMES experiment is therefore a good example of the potential bias shown in Fig. 6. In the numerical simulation of DIMES, 7% of the tracer ended up within 1000 m off the bottom, where mixing was two orders of magnitude above background values, but occupied less than 1% of the area. The strong correlation between large  $\kappa$  and cresulted in  $K_{\text{Taylor}} \gg \kappa$ . The  $K_{\omega}$  played less of a role, because the zonal flow advected the tracer above seamounts and ridges, too close to the seafloor to develop much skewness toward denser waters. While the analysis of Mashayek et al. (2017) was quite heuristic, our formulas put their results on solid theoretical footing.

Finally, our analysis suggests that vertical and horizontal variations in turbulent mixing may explain why diffusivity estimates based on TREs tend to exceed those based on microstructure measurements. However, a similar bias has also been reported from observations in regions where mixing was supposedly quite uniform. Both in the North Atlantic Tracer Release Experiment (NATRE) which targeted the main thermocline west of the Canary Islands (Ledwell et al. 1998) and in the aformentioned DIMES experiment, but west of Drake Passage, the TRE based estimates of diffusivity exceeded those from microstructure measurements. It is possible that small variations in mixing rates played a role, but we cannot exclude additional unknown effects.

#### 6. Conclusions

We extended Taylor's formula that quantitatively relates the spreading of a tracer to the rate of turbulent mixing. The new formulas in Eqs. (9) and (10) include the impact of variations in stratification and mixing rates, which are key aspects of ocean turbulence. A major insight is that the spreading of the tracer across ocean density surfaces is not only proportional to the magnitude of the diapycnal diffusivity  $\kappa$  but also to 1) vertical variations in buoyancy flux divergence  $\omega = \partial_z(\kappa \partial_z b)$  and 2) correlations between  $\kappa$ ,  $\omega$ , stratification and the tracer concentration. The former effect is particularly important in the abyss, over rough bathymetry, where the buoyancy flux rapidly increases toward the seafloor. Such a profile results in a diapycnal velocity  $\omega$  increasing toward the ocean bottom and acting to stretch the tracer cloud toward higher densities, as illustrated in our idealized simulations and reported in observations (Ledwell et al. 2000). The latter effect is also significant, because, in the absence of along-isopycnal advection, tracers tend to accumulate in regions of large  $\kappa$  and  $\omega$ . This would result in a positive correlation between  $\kappa$  and the tracer concentration and accelerates the tracer spreading compared to an environment with constant  $\kappa$ . Correlations between  $\kappa$  and

<sup>&</sup>lt;sup>3</sup> Ledwell replaced the two-parameter analytical function for K(z) in the one-dimensional advection—diffusion equation with a self-similar function as a function of height above the bottom. Following Mashayek et al. (2017), a 3D diffusivity map was created by assuming the self-similar profile in Eq. (11) with z representing the height above the local bottom. The map varied in all three dimensions, because the profiles were shifted up and down depending on the local bathymetry. A 1D diffusivity profile K(z) was then obtained by averaging the 3D map along isopycnals within the region occupied by the tracer. The parameters in the self-similar function (11) were chosen to obtain the best fit to the tracer distribution measured at 14 months.

 $<sup>^4</sup>$  Watson et al. (2013) used a slightly more general formulation where u had a vertical shear and there was a constant horizontal diffusion term, but these embellishments had very minor influence on the final estimate.

stratification have also been shown to arise in field experiments (Ledwell et al. 2000; Mashayek et al. 2017; Wagner et al. 2019).

The traditional approach to estimate diapycnal velocity and diffusivity from TREs has been solving a 1D advection—diffusion equation that best matches the observed evolution of the along-isopycnal-averaged tracer distribution. Second moments in the vertical (or in density space) are rarely used because they provide only bulk estimates over the whole tracer volume. While it is true that the 1D approach addresses vertical variations in mixing rate, it does not account for the horizontal (technically along isopycnal) biases. Our review of two seminal tracer release experiments suggests that lateral correlations between tracer concentration and mixing intensity can substantially increase the net mixing experienced by oceanic tracers.

Most importantly our formulas offer insights on the longstanding conundrum of why diapycnal diffusivity required to close basin-scale tracer budgets (Hogg et al. 1982; Whitehead and Worthington 1982; Heywood et al. 2002; Voet et al. 2015) are often much larger than those measured with in situ microstructure probes. In these budgets a diapycnal diffusivity is estimated to balance the flux of tracer into a density class. This value is then compared to the rate of turbulent mixing measured across the same density surface with microstructure probes. The discrepancy between the two estimates is generally attributed to rare localized mixing hotspots that are easily missed by microstructure profiles. Our formulas show that no such hotspots are needed to explain these differences. Both vertical gradients in diapycnal diffusivities and correlations between turbulent mixing, density stratification and tracer concentration can substantially enhance the mixing experienced by a tracer compared to in situ turbulent measurements.

Acknowledgments. We thank Jim Ledwell, Jörn Callies, Kurt Polzin, Kelly Ogden, and Henri Drake for helpful discussions. Support through NSF Awards OCE-1736109 and OCE-1756324 is gratefully acknowledged.

#### APPENDIX A

## Derivation of the Evolution Equations of the Tracer-Weighted Buoyancy Moments

Multiplying Eq. (3) by buoyancy b and Eq. (4) by tracer concentration c and summing up the results, an evolution equation for the product (bc) can be written as

$$\partial_{s}(bc) + \mathbf{u} \cdot \nabla(bc) = \nabla \cdot (b\kappa \nabla c - c\kappa \nabla b) + 2c\nabla \cdot (\kappa \nabla b).$$
 (A1)

Integrating this equation over the full ocean and assuming that the tracer concentration vanishes at infinity or the tracer and buoyancy fluxes vanish at the boundaries, we obtain Eq. (6). The second term on the left hand side can be rewritten as

$$\mathbf{u} \cdot \nabla(bc) = \nabla \cdot (\mathbf{u}bc) - bc\nabla \cdot \mathbf{u}, \tag{A2}$$

which vanishes after the integral and under the incompressibility assumption. Similarly, an evolution equation for  $cb^2$  can be obtained as

$$\partial_{t}(cb^{2}) + \mathbf{u} \cdot \nabla(cb^{2}) = \nabla \cdot (\kappa b^{2} \nabla c - \kappa c \nabla b^{2}) + 2\kappa |\nabla b|^{2} c + 4bc \nabla \cdot (\kappa \nabla b). \tag{A3}$$

Again, Eq. (7) can be derived after integrating the equation above over the whole ocean volume and imposing the no-flux boundary conditions.

#### APPENDIX B

#### **Details about the Numerical Simulations**

The numerical simulations are performed using the Massachusetts Institute of Technology general circulation model (MITgcm) in a doubly periodic rectangular box with a flat bottom. The domain size is 100 km in the horizontal directions and 2000 m in the vertical. The numerical integration is evolved with a 200-s time step. The simulations are run in two steps: 1) a spinup experiment for 220 days with a uniform  $\kappa = 2 \times 10^{-5} \, \mathrm{m^2 \, s^{-1}}$  as well as a constant stratification ( $N^2 = 1 \times 10^{-6} \, \mathrm{s^{-2}}$ ) with an initial sinusoidal buoyancy perturbation in the *y* direction for the mesoscale eddy field to develop, and 2) two experiments with numerical tracer release are performed for 180 days. A sponge layer (400 m thick) is embedded at the bottom with a restoring time of one hour. The initial tracer distribution follows a 3D Gaussian profile:

$$c_0(x, y, z) = \exp\left\{-\left[\frac{(x - x_0)^2}{(2\sigma_x^2)} + \frac{(y - y_0)^2}{(2\sigma_y^2)} + \frac{(z - z_0)^2}{(2\sigma_z^2)}\right]\right\},\,$$

where  $x_0 = y_0 = 50 \,\mathrm{km}$  (in the middle of the domain) and  $z_0 = 1100 \,\mathrm{m}$ . Experiment A employs a constant  $\kappa = 2 \times 10^{-5} \,\mathrm{m}^2 \,\mathrm{s}^{-1}$  and experiment B applies a bottom-intensified diffusivity profile as a function of height above the bottom (Fig. 2a):

$$\kappa = 2 \times 10^{-5} + 1.8 \times 10^{-3} e^{-z/(230 \text{m})} \text{ m}^2 \text{ s}^{-1}$$
.

where the bottom is at z=0. The sponge layer is needed in order to maintain the near-bottom stratification, otherwise a bottom mixed layer of order hundreds of meters would develop with the near-bottom stratification much weaker than observed. The sponge layer introduces extra spurious buoyancy sources/sinks, thus we choose  $1600 \, \text{m}$  as the "bottom" for our local height above the bottom (HAB) coordinate away from the sponge layer and the tracers are released at  $1100 \, \text{m}$  (thus at  $500 \, \text{m}$  HAB). We do not show the results below  $1600 \, \text{m}$  and there is no tracer that is mixed below  $1600 \, \text{m}$ .

#### APPENDIX C

## Comparison of Skewness in Depth and Buoyancy Spaces

Following Taylor (1922) and similar approaches used in this study, we can write the evolution of the first and second moments of the tracer distribution in depth space as

$$\partial_{\tau}\overline{z} = \overline{\partial_{z}\kappa},$$
 (C1)

$$\partial_t \overline{z^2} = 2\overline{\kappa} + 2\overline{z}\partial_z \kappa, \tag{C2}$$

where only the vertical component is used to approximate the full 3D gradients. The evolution of the centered second moment can thus be written as

$$\partial_t \overline{(z - \overline{z})^2} = 2\overline{\kappa} + 2\left(\overline{z}\partial_z \kappa - \overline{\partial}_z \kappa \overline{z}\right). \tag{C3}$$

As derived in the main text, the evolution of the centered second moment in buoyancy space is

$$\partial_{t} \overline{(b - \overline{b})^{2}} = 2 \overline{\kappa (\partial_{z} b)^{2}} + 4 \overline{b \partial_{z} (\kappa \partial_{z} b)} - \overline{\partial_{z} (\kappa \partial_{z} b)} \overline{b}. \quad (C4)$$

To make the comparison clearer, we assume  $b_z$  is a constant and Eq. (C4) can be rearranged as

$$\frac{\partial_{t} \overline{(b-\overline{b})^{2}}}{\left(\partial_{z} b\right)^{2}} = 2\overline{\kappa} + 4\left(\frac{\overline{b}\partial_{z}\kappa - \overline{\partial_{z}\kappa}\overline{b}}{\partial_{z}b}\right). \tag{C5}$$

From comparing Eqs. (C3) and (C5), the skewness induced by vertical variation in  $\kappa$  in depth space is half of that induced by vertical variation in  $\omega$  in buoyancy space. The comparison is more complicated when variation in stratification is introduced.

#### REFERENCES

- Callies, J., and R. Ferrari, 2018: Dynamics of an abyssal circulation driven by bottom-intensified mixing on slopes. *J. Phys. Oceanogr.*, 48, 1257–1282, https://doi.org/10.1175/JPO-D-17-0125.1.
- de Lavergne, C., G. Madec, J. Le Sommer, A. G. Nurser, and A. C. Naveira Garabato, 2016: On the consumption of Antarctic bottom water in the abyssal ocean. *J. Phys. Oceanogr.*, 46, 635–661, https://doi.org/10.1175/JPO-D-14-0201.1.
- Ferrari, R., 2014: What goes down must come up. *Nature*, **513**, 179–180, https://doi.org/10.1038/513179a.
- —, and C. Wunsch, 2009: Ocean circulation kinetic energy: Reservoirs, sources, and sinks. *Annu. Rev. Fluid Mech.*, 41, 253–282, https://doi.org/10.1146/annurev.fluid.40.111406.102139.
- —, A. Mashayek, T. J. McDougall, M. Nikurashin, and J.-M. Campin, 2016: Turning ocean mixing upside down. J. Phys. Oceanogr., 46, 2239–2261, https://doi.org/10.1175/JPO-D-15-0244.1.
- Heywood, K. J., A. C. N. Garabato, and D. P. Stevens, 2002: High mixing rates in the abyssal Southern Ocean. *Nature*, 415, 1011– 1014, https://doi.org/10.1038/4151011a.
- Hogg, N., P. Biscaye, W. Gardner, and W. J. Schmitz Jr., 1982: On the transport and modification of Antarctic bottom water in the Vema channel. J. Mar. Res., 40, 231–263.
- Holmes, R., C. de Lavergne, and T. J. McDougall, 2019: Tracer transport within abyssal mixing layers. J. Phys. Oceanogr., 49, 2669–2695, https://doi.org/10.1175/JPO-D-19-0006.1.
- Jackett, D. R., and T. J. McDougall, 1997: A neutral density variable for the world's oceans. J. Phys. Oceanogr., 27, 237–263, https://doi.org/10.1175/1520-0485(1997)027<0237:ANDVFT> 2.0.CO;2.
- Klocker, A., and T. J. McDougall, 2010: Influence of the nonlinear equation of state on global estimates of dianeutral advection and diffusion. *J. Phys. Oceanogr.*, 40, 1690–1709, https:// doi.org/10.1175/2010JPO4303.1.
- Ledwell, J. R., and A. Bratkovich, 1995: A tracer study of mixing in the Santa Cruz Basin. J. Geophys. Res., 100, 20681–20704, https://doi.org/10.1029/95JC02164.

- ——, A. J. Watson, and C. S. Law, 1998: Mixing of a tracer in the pycnocline. *J. Geophys. Res.*, **103**, 21499–21529, https:// doi.org/10.1029/98JC01738.
- ——, E. Montgomery, K. Polzin, L. S. Laurent, R. Schmitt, and J. Toole, 2000: Evidence for enhanced mixing over rough topography in the abyssal ocean. *Nature*, **403**, 179–182, https:// doi.org/10.1038/35003164.
- Lumpkin, R., and K. Speer, 2007: Global ocean meridional overturning. J. Phys. Oceanogr., 37, 2550–2562, https://doi.org/ 10.1175/JPO3130.1.
- Marshall, J., and T. Radko, 2003: Residual-mean solutions for the Antarctic Circumpolar Current and its associated overturning circulation. *J. Phys. Oceanogr.*, 33, 2341–2354, https://doi.org/10.1175/1520-0485(2003)033<2341:RSFTAC> 2.0.CO:2.
- —, and K. Speer, 2012: Closure of the meridional overturning circulation through Southern Ocean upwelling. *Nat. Geosci.*, 5, 171–180, https://doi.org/10.1038/ngeo1391.
- —, A. Adcroft, C. Hill, L. Perelman, and C. Heisey, 1997: A finite-volume, incompressible Navier Stokes model for studies of the ocean on parallel computers. *J. Geophys. Res.*, 102, 5753–5766, https://doi.org/10.1029/96JC02775.
- Mashayek, A., R. Ferrari, S. Merrifield, J. Ledwell, L. St Laurent, and A. N. Garabato, 2017: Topographic enhancement of vertical turbulent mixing in the Southern Ocean. *Nat. Commun.*, 8, 14197, https://doi.org/10.1038/ ncomms14197.
- Munk, W. H., 1966: Abyssal recipes. Deep-Sea Res., 13, 707–730, https://doi.org/10.1016/0011-7471(66)90602-4.
- Osborn, T. R., 1980: Estimates of the local rate of vertical diffusion from dissipation measurements. *J. Phys. Oceanogr.*, **10**, 83–89, https://doi.org/10.1175/1520-0485(1980)010<0083: EOTLRO>2.0.CO;2.
- —, and C. Cox, 1972: Oceanic fine structure. *Geophys. Fluid Dyn.*, **3**, 321–345, https://doi.org/10.1080/03091927208236085.
- Polzin, K. L., 2009: An abyssal recipe. *Ocean Modell.*, 30, 298–309, https://doi.org/10.1016/j.ocemod.2009.07.006.
- —, J. Toole, J. Ledwell, and R. Schmitt, 1997: Spatial variability of turbulent mixing in the abyssal ocean. *Science*, 276, 93–96, https://doi.org/10.1126/science.276.5309.93.
- St. Laurent, L. C., A. C. Naveira Garabato, J. R. Ledwell, A. M. Thunherr, J. M. Toole, and A. J. Watson, 2012: Turbulence and diapycnal mixing in Drake Passage. J. Phys. Oceanogr., 42, 2143–2152, https://doi.org/10.1175/JPO-D-12-027.1.
- Stommel, H., and A. Arons, 1959: On the abyssal circulation of the world ocean—I. Stationary planetary flow patterns on a sphere. *Deep-Sea Res.*, **6**, 140–154, https://doi.org/10.1016/0146-6313(59)90065-6.
- Talley, L. D., 2013: Closure of the global overturning circulation through the Indian, Pacific, and Southern Oceans: Schematics and transports. *Oceanography*, 26, 80–97, https://doi.org/ 10.5670/oceanog.2013.07.
- Taylor, G. I., 1922: Diffusion by continuous movements. Proc. London Math. Soc., s2–20, 196–212, https://doi.org/10.1112/ plms/s2-20.1.196.
- Voet, G., J. B. Girton, M. H. Alford, G. S. Carter, J. M. Klymak, and J. B. Mickett, 2015: Pathways, volume transport, and mixing of abyssal water in the Samoan passage. *J. Phys. Oceanogr.*, 45, 562–588, https://doi.org/10.1175/JPO-D-14-0096.1.
- Wagner, G. L., G. Flierl, R. Ferrari, G. Voet, G. S. Carter, M. H. Alford, and J. B. Girton, 2019: Squeeze dispersion and the effective diapycnal diffusivity of oceanic tracers.

- Geophys. Res. Lett., 46, 5378–5386, https://doi.org/10.1029/2019GL082458.
- Waterhouse, A. F., and Coauthors, 2014: Global patterns of diapycnal mixing from measurements of the turbulent dissipation rate. J. Phys. Oceanogr., 44, 1854–1872, https://doi.org/10.1175/JPO-D-13-0104.1.
- Watson, A. J., J. R. Ledwell, M.-J. Messias, B. A. King, N. Mackay, M. P. Meredith, B. Mills, and A. C. N. Garabato, 2013: Rapid cross-density ocean mixing at mid-depths in the drake passage
- measured by tracer release. *Nature*, **501**, 408–411, https://doi.org/10.1038/nature12432.
- Whitehead, J., Jr., and L. Worthington, 1982: The flux and mixing rates of Antarctic Bottom Water within the North Atlantic. *J. Geophys. Res.*, **87**, 7903–7924, https://doi.org/10.1029/JC087iC10p07903.
- Wunsch, C., 2017: Ocean mixing. Oxford Encyclopedia of Climate Science, H. Von Storch, Ed., Oxford University Press, https:// doi.org/10.1093/acrefore/9780190228620.013.90.